A Framework for Intrinsic Image Processing on Surfaces

Rongjie Lai, T. F. Chan

Department of Mathematics, UCLA, Los Angeles, CA 90095, USA

Abstract

After many years of study, the subject of image processing on the plane, or more generally in Euclidean space is well developed. However, more and more practical problems in different areas inspire us to consider imaging on surfaces beyond imaging on Euclidean domains. Several approaches, such as implicit representation approaches and parametrization approaches, are investigated about image processing on surfaces. Most of these methods require certain preprocessing to convert image problems on surfaces to image problems in Euclidean spaces. In this work, we use differential geometry techniques to directly study image problems on surfaces. By using our approach, all plane image variation models and their algorithms can be naturally adapted to study image problems on surfaces. As examples, we show how to generalize Rudin-Osher-Fatemi (ROF) denoising model [39] and convexified Chan-Vese (CV) [10] segmentation model on surfaces, and then demonstrate how to use popular algorithms to solve the total variation related problems on surfaces. This intrinsic approach provides us a robust and efficient method to directly study image processing, and in particular, total variation problems on surfaces without requiring any preprocessing.

Keywords: differential geometry, surface imaging, total variation, image denoising, image segmentation.

1. Introduction

The variational method in image processing is quite an important approach. After decades of development, many beautiful results are explored, such as variational models of image denosing, image inpainting, image segmentation [39, 12, 11, 10, 13] etc. However, most results focus on image processing in Euclidean space, in particular, image processing on the 2D plane.

With the development of 3D data acquisition technology and the requirement of various applications, there has been increasing interest in studying image processing and variational problems on surfaces or general manifolds. For instance, in fields like computer vision, computer graphics, geometry modeling, medical imaging, computational anatomy, geo-physics and 3D cartoon, it is critical to consider images on 3D surfaces instead of images only on 2D planes.

Several approaches are explored to study image processing on surfaces by using the variational PDE method. To the best of our knowledge, there are, roughly speaking, two classes of approaches to study surfaces imaging, which reflect two different surface representations. One class is using implicit representation of surfaces. S. Osher, G. Sapiro, M. Bertalmio, L. T. Cheng et al. [5, 29, 4, 36, 7] view a closed surface as a zero level set of a signed distance function on a Euclidean domain or a narrow band of the given surface. They approximate differential operators on surfaces by combining the standard Euclidean differential operators with projection along the normal direction. The biggest advantage of implicit representation of surfaces is that one can easily handle topological changes under surface evolution. However, it has its own limitations. For instance, fast algorithms in Euclidean cases can not be easily adapted to surface cases by implicit method; For open surfaces, or surfaces with complicated structures, like human's cortical surfaces with many close and deep folding parts, it is not easy to obtain their implicit representations. In addition, the cost of the implicit representations is the pre-step to extend all data on the definition domain of implicit function. These additional increasing data might decrease the computation speed. Another class is using explicit representation of surfaces, namely, surfaces are represented by polygon meshes, in particular, triangle meshes. J. Stam, L. Lopez-Perez, X. Gu, L. Lui et al. [41, 32, 28, 33] introduce either standard patch-wise parametrization or conformal parametrization to the given surface, then differential operators can be computed under the corresponding parametrization. However, the computation of a parametrization is a complicated pre-processing for arbitrary given surfaces, especially for those surfaces with complicated structures or high genus. To conclude, the above methods mainly focus on converting problems on surfaces to problems in Euclidean space. They require pre-processing, either extending data to the narrow band of the given surface or finding a parametrization of the given surface.

Our strategy is different from the above methods. To avoid the need for pre-processing, we will focus on studying variational imaging models directly on the given surface instead of converting them to be problems in Euclidean spaces. Specially, we take two well-known models, namely the ROF denoising model and the CV segmentation model, as examples to explain our strategy. Related work and applications of the intrinsic geometry method can be found in a series work of M. Meyer, M. Desbrun, P. Schroder, A. Barr, G. Xu, C. Bajaj and U. Clarenz, et al. [37, 19, 2, 42, 16]. However, our contribution in this work is using intrinsic geometry method to study the total variation related image processing problems on surfaces and fast algorithms. The most natural extension of the total variation (TV) on surfaces, which is also well-defined on any n-dimensional manifold, is given by M. Ben-Artzi and P. G. LeFloch in [3]. By their natural definition of the total variation on surfaces, we prove the analogous boundary perimeter formula and co-area formula of TV on surfaces, which illustrate the suitability of using TV to study image processing on surfaces. After this, we generalize the ROF denosing model and the CV segmentation model on surfaces as two examples. To implement the above models on triangulated surfaces, we approximate surface gradient and divergence operators by using their intrinsic differential geometry definition. Furthermore, we represent the action of these operators as the multiplication of sparse matrix to simplify our computation. As a consequence of this intrinsic geometry method, we can easily adapt many well-known algorithms in the total variation related problems in Euclidean cases to the generalization total variation image models on surfaces. As examples, we discuss the split Bregman iteration method [27, 26] and Chambolle's dual method [9, 6] on surfaces. In our experience, there are at least two advantages of our intrinsic method. First, we do not need to conduct pre-processing, such as extending all data on the narrow band in the implicit representation or finding a good parametrization in explicit representation. For instance, in the implicit method, when we process high resolution data, like a cortical surface, dealing with large amount of additional data will waste too much computation time; in the parametrization method, when we process surfaces with complicated structures, it is not easy to obtain a good parametrization. Our direct method can be expected to overcome these limitations. In addition, fast algorithms in Euclidean cases can be easily adapted to solve the total variational problems on surfaces due to the intrinsic method. Second, by this intrinsic method, it is easy to handle open surfaces and surfaces with complicated geometric or topological structures, which can not be easily processed by implicit methods or parametrization methods. A brief comparison among different methods is given in the Table 1. To explain everything

method	principle	Advantage	Disadvantage
level set representation	view a surface as a zero level set of a function	easy to handle topological changes when dealing with surface evolution	all data need to be extended to the narrow band of surface, hard to adapt fast algorithms in Euclidean cases
parametrization method	parameterize patches of a surface by Euclidean coordinates	differential operators are easy to compute after finding parametrization	not easy to obtain parametrization for an arbitrary surface, hard to handle topological change
intrinsic geometry method	computation processed on the given surface itself by differential geometry techniques	can deal with any surface without any preprocessing, easy to adapt fast algorithms in Euclidean cases	hard to handle topological changes

Table 1: comparison among different methods

clearly, we are here just focusing on closed surface cases. One can also study open surfaces with this general technique.

The rest of the paper is organized as follows. In Section 2, we give a brief review of the intrinsic definition of gradient, divergence and Laplace-Beltrami operators on a given surface, then provide their discretization and sparse matrix representations. After that, in Section 3, we first generalize the concept of TV on surfaces, and demonstrate the analogous version of the boundary perimeter formula and co-area formula for TV on surfaces. Then, we introduce a general form of variational models on surfaces and take the ROF denoising model, the total variational inpainting model, the CV segmentation model as examples to show how to generalize variational models of image processing on planes to variational models of image processing on surfaces. The numerical algorithms of ROF denoising and CV segmentation on surfaces are then presented in Section 4. In particular, we use the split Bregman iteration and the dual method on surfaces to solve above models on surfaces. Numerical comparisons with the conformal parametrization method and the level set method are given in Section 5. Meanwhile, we demonstrate applications of surface image denoising to geometric processing and surface image segmentation to cortical surface parcellation in computational anatomy. Finally, conclusions are made in Section 6.

2. Background of Differential Geometry

To generalize image processing on surfaces, it is necessary to involve the geometry of the ground surface in the processing. Fortunately, standard differential geometry provides us a natural way to handle surface geometry. Therefore, we would like to review a little bit of differential geometry concepts before we discuss image processing on surfaces. In this section, we will introduce the intrinsic definition of gradient, divergence and Laplace-Beltrami operators on a given surface, then we will discuss their discretization and sparse matrix representation.

2.1. Differential operators on surfaces

Let (M, g) be a two dimensional closed Riemannian manifold. For any point $p \in M$ and its local coordinate chart $\{U, x = (x^1, x^2)\}$, we can represent the metric $g(p) = (g_{ij}(x))_{i,j=1,2}$. Then, one can define the surface gradient, divergence, and Laplacian-Beltrami operators as the following:

$$\nabla_M f = \sum_{i,j=1}^{2} g^{ij} \frac{\partial f}{\partial x^i} \partial_{x^j} \tag{1}$$

$$\mathrm{div}_M \mathbb{V} = \frac{1}{\sqrt{G}} \sum_{i=1}^{2} \frac{\partial}{\partial x^i} (\sqrt{G} v^i), \text{ for } \mathbb{V} = \sum_{i=1}^{2} v^i \partial_{x^i} \tag{2}$$

$$\triangle_M f = \mathrm{div}_M(\nabla_M f) = \frac{1}{\sqrt{G}} \sum_{i=1}^{2} \frac{\partial}{\partial x_i} (\sqrt{G} \sum_{j=1}^{2} g^{ij} \frac{\partial f}{\partial x_j}) \tag{3}$$

where (g^{ij}) is the inverse matrix of (g_{ij}) and $G = \det(g_{ij})$.

For any two functions $f, g : M \to \mathbb{R}$, and any tangent vector field $\mathbb{V} = \sum_{i=1}^{2} v^i \frac{\partial}{\partial x^i}$, the divergence theorems on surfaces similar as in $\mathbb{R}^n$ can be describe by:

$$\int_M (\mathrm{div}_M \mathbb{V}) f \mathrm{d}s = -\int_M \mathbb{V} \cdot \nabla_M f \mathrm{d}s \tag{4}$$

$$\int_M (\triangle_M f) g \mathrm{d}s = -\int_M \nabla_M f \cdot \nabla_M g \mathrm{d}s \tag{5}$$

Details about the above differential geometry concepts can be obtained in many textbook on differential geometry, for example [31].

Moreover, one can define the l^1 and l^2 norm, respectively, as follows:

$$||f||_1 = \int_M |f| \mathrm{d}s, \quad ||f||_2 = (\int_M f^2 \mathrm{d}s)^{1/2}, \quad \langle f, g \rangle = \int_M fg \mathrm{d}s \tag{6}$$

$$|\mathbb{V}| = (\sum_{i,j=1}^{2} g_{ij} v^i v^j)^{1/2}, \quad ||\mathbb{V}||_1 = \int_M |\mathbb{V}| \mathrm{d}s, \quad ||\mathbb{V}||_2 = \int_M |\mathbb{V}|^2 \mathrm{d}s, \tag{7}$$

2.2. Discretization of differential operators

With the mathematical definition of differential operators given above, we can consider their numerical approximation in a discrete data setting. The surface data structure we focus on is the triangle mesh surface representation. Namely, given surface M in $\mathbb{R}^3$, it is represented as a triangle mesh $M = \{P = \{p_i\}_{i=1}^N, T = \{T_l\}_{l=1}^L\}$, where $p_i \in \mathbb{R}^3$ is the i-th vertex and $T_l \in \mathbb{N}^3$ represents indices of three vertices of the l-th triangle. Since the definition of surface gradient, divergence operator are pointwise, we can consider the pointwise first order numerical approximation of them in the first ring of each vertex. The idea of our approximation can be realized as two steps. We first compute the discretization on each triangle by their definition given in (1),(2), then take a weighted average in the first ring of each of the vertex in terms of the neighbor triangle areas.

First of all, we show the operators discretization on a given triangle $T_l = \{p_0, p_1, p_2\}$. In the discrete case, we have a function $f = \{f(p_0), f(p_1), f(p_2)\}$ and a vector field $\mathbb{V} = \{\mathbb{V}(p_0), \mathbb{V}(p_1), \mathbb{V}(p_2)\}$ defined on each vertex respectively. With the barycentric coordinates $\{(x^1, x^2, 1 - x^1 - x^2) \mid 0 \leqslant x^1, x^2, x^1 + x^2 \leqslant 1\}$ of T_l, any point $p \in T_l$, the linear interpolation of $f, \mathbb{V}$ in T_l can be given by:

$$\begin{cases} p = x^1(p_1 - p_0) + x^2(p_2 - p_0) + p_0 \\ f(p) = x^1(f(p_1) - f(p_0)) + x^2(f(p_2) - f(p_0)) + f(p_0) \\ \mathbb{V}(p) = x^1(\mathbb{V}(p_1) - \mathbb{V}(p_0)) + x^2(\mathbb{V}(p_2) - \mathbb{V}(p_0)) + \mathbb{V}(p_0) \end{cases} \tag{8}$$

Then we have $\partial_{x^1} = p_1 - p_0, \partial_{x^2} = p_2 - p_0$, and the metric matrix of T_l would be:

$$g = (g_{i,j})_{i,j=1,2} = \begin{pmatrix} \partial_{x^1} \cdot \partial_{x^1} & \partial_{x^1} \cdot \partial_{x^2} \\ \partial_{x^2} \cdot \partial_{x^1} & \partial_{x^2} \cdot \partial_{x^2} \end{pmatrix} \text{ and } (g^{i,j})_{i,j=1,2} = g^{-1} \tag{9}$$

where $\cdot$ is the dot product in $\mathbb{R}^3$. We then have the following discretization:

$$\nabla_{T_l}^d f(p_0) = \sum_{i,j=1}^{2} g^{ij} \frac{\partial f}{\partial x^j} \partial_{x^i} = (f(p_1) - f(p_0), f(p_2) - f(p_0)) g^{-1} \begin{pmatrix} \partial_{x^1} \\ \partial_{x^2} \end{pmatrix}$$

$$= (f(p_1) - f(p_0), f(p_2) - f(p_0)) \begin{pmatrix} \partial_{x^1} \cdot \partial_{x^1} & \partial_{x^1} \cdot \partial_{x^2} \\ \partial_{x^2} \cdot \partial_{x^1} & \partial_{x^2} \cdot \partial_{x^2} \end{pmatrix}^{-1} \begin{pmatrix} p_1 - p_0 \\ p_2 - p_0 \end{pmatrix} \tag{10}$$

We next discretize the divergence operator on the triangle T_l. Suppose $\mathbb{V} = v_1 \partial_{x^1} + v_2 \partial_{x^2}$ is a vector field on T_l. Then the coefficients v^1, v^2 are given by:

$$\begin{pmatrix} v_1 \\ v_2 \end{pmatrix} = g^{-1} \begin{pmatrix} \mathbb{V} \cdot \partial_{x^1} \\ \mathbb{V} \cdot \partial_{x^2} \end{pmatrix} \tag{11}$$

Differentiate both sides of above equality, we have:

$$\begin{pmatrix} \frac{\partial}{\partial x^1} v_1 \\ \frac{\partial}{\partial x^2} v_2 \end{pmatrix} = \begin{pmatrix} g^{11}(\mathbb{V}(p_1) - \mathbb{V}(p_0)) \cdot \partial_{x^1} + g^{12}(\mathbb{V}(p_1) - \mathbb{V}(p_0)) \cdot \partial_{x^2} \\ g^{21}(\mathbb{V}(p_2) - \mathbb{V}(p_0)) \cdot \partial_{x^1} + g^{22}(\mathbb{V}(p_2) - \mathbb{V}(p_0)) \cdot \partial_{x^2} \end{pmatrix} \tag{12}$$

Since $\sqrt{G}$ is constant on each triangle, we can obtain the discretization of the divergence operator on triangle T_l by directly using its definition in (2)

$$\mathrm{div}^d_{T_l} \mathbb{V}(p_0) = \frac{1}{\sqrt{G}} \sum_{i=1}^{2} \frac{\partial}{\partial x^i}(\sqrt{G} v^i) = \frac{\partial}{\partial x^1}(v_1) + \frac{\partial}{\partial x^2}(v_2) \tag{13}$$

Now, we can discuss the discretization of the gradient and divergence operators at each vertex by taking a weighted average in the first ring of each vertex in terms of triangle areas. Namely, for any function f and vector field $\mathbb{V}$ defined on triangle mesh $\{V = \{p_i\}_{i=1}^N, T = \{T_l\}_{l=1}^L\}$, we use the following discretization of gradient and divergence operators:

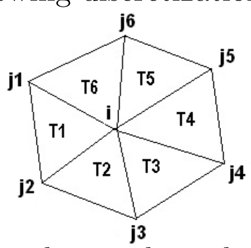

$$\nabla^d_M f(p_i) = \frac{1}{\sum_l Area(T_l)} \sum_l Area(T_l) \nabla^d_{T_l} f(p_0) \tag{14}$$

$$\mathrm{div}^d_M \mathbb{V}(p_i) = \frac{1}{\sum_l Area(T_l)} \sum_l Area(T_l) \mathrm{div}^d_{T_l} \mathbb{V}(p_0) \tag{15}$$

where l goes through all triangles in the first ring of p_i as showed in above figure.

In the rest of the paper, we will also use ∇_M, and div_M to denote their discretization operators respectively.

Remark 1. *We need to point out that we are not the first group to consider similar discretization of surface gradient and divergence. Other different discretization methods and their approximation analysis can be found in a series works of M. Meyer, M. Desbrun, P. Schroder, A. Barr and G.Xu et.al*

[37, 19, 42]. In this paper, our contribution is using above discrete differential geometry technique to solve variational problems on surfaces, especially the total variation models and their related image processing problems. In Section 4.3, We will use finite element to compute surface Laplacian to avoid approximating the second order operators. Therefore, we just need to approximate gradient and divergence operators.

2.3. Sparse matrix representations of differential operators

With above discretization of differential operators, one can compute the gradient and divergence on any surface. In addition, we observe that one can write down the sparse matrix representations of gradient and divergence. Namely, these two surface differential operators can be realized as matrix multiplications. It turns out that the computation speed can be improved a lot with the sparse matrix representations of differential operators. In principle, all linear operators on surface can be written as matrix multiplications with similar technique.

Before we discuss the sparse representations of differential operators, we would like to introduce some notation as follows:

We write $\overrightarrow{C} = (\overrightarrow{c_{ij}}), \overrightarrow{D} = (\overrightarrow{d_{ij}})$ as a vector matrix, i.e. each entry of $\overrightarrow{C}$, $\overrightarrow{D}$ is a vector in $\mathbb{R}^3$ instead of a number, let $A = (a_{ij})$ be a number matrix as usual and λ be a real number. We define the following multiplications:

$$(\lambda\overrightarrow{D})_{ij} = \lambda\overrightarrow{d_{ij}}, \quad (\overrightarrow{D}A)_{ij} = \sum_k \overrightarrow{d_{ik}} a_{kj} \tag{16}$$

$$(\overrightarrow{C} \bullet \overrightarrow{D})_{ij} = \sum_k \overrightarrow{c_{ik}} \cdot \overrightarrow{d}_{kj}, \quad (\overrightarrow{C} \times \overrightarrow{D})_{ij} = \sum_k \overrightarrow{c_{ik}} \times \overrightarrow{d}_{kj} \tag{17}$$

where $\cdot, \times$ in the right hand side is the standard dot, cross product in $\mathbb{R}^3$ respectively.

We first write down the matrix representation of gradient and divergence on each triangle. From (10) and (13), we have:

$$\begin{aligned} \nabla_{T_l} f(p_0) = {} & g^{11}(f(p_1) - f(p_0))\partial_{x^1} + g^{12}(f(p_1) - f(p_0))\partial_{x^2} \\ & + g^{21}(f(p_2) - f(p_0))\partial_{x^1} + g^{22}(f(p_2) - f(p_0))\partial_{x^2} \end{aligned} \tag{18}$$

$$\begin{aligned} \mathrm{Div}_{T_l}\mathbb{V}(p_0) = {} & g^{11}(\mathbb{V}(p_1) - \mathbb{V}(p_0)) \cdot \partial_{x^1} + g^{12}(\mathbb{V}(p_1) - \mathbb{V}(p_0)) \cdot \partial_{x^2} \\ & + g^{21}(\mathbb{V}(p_2) - \mathbb{V}(p_0)) \cdot \partial_{x^1} + g^{22}(\mathbb{V}(p_2) - \mathbb{V}(p_0)) \cdot \partial_{x^2} \end{aligned} \tag{19}$$

Remember $\partial_{x^1} = p_1 - p_0$ and $\partial_{x^2} = p_2 - p_0$. If we write

$$\left\{\begin{array}{l} \overrightarrow{w}_{T_l}^{p_0} = -(g^{11}+g^{21})(p_1-p_0) - (g^{12}+g^{22})(p_2-p_0) \\ \overrightarrow{w}_{T_l}^{p_1} = g^{11}(p_1-p_0) + g^{12}(p_2-p_0) \\ \overrightarrow{w}_{T_l}^{p_2} = g^{21}(p_1-p_0) + g^{22}(p_2-p_0) \\ \overrightarrow{W}_{T_l} = (\overrightarrow{w}_{T_l}^{p_0}, \overrightarrow{w}_{T_l}^{p_1}, \overrightarrow{w}_{T_l}^{p_2}) \\ f_{T_l} = (f(p_0), f(p_1), f(p_2))^t \\ \mathbb{V}_{T_l} = (\mathbb{V}(p_0), \mathbb{V}(p_1), \mathbb{V}(p_2))^t \end{array}\right. \tag{20}$$

then we have,

$$\left\{\begin{array}{l} \nabla_{T_l} f(p_0) = \overrightarrow{W}_{T_l} f_{T_l} \\ \mathrm{div}_{T_l}\mathbb{V}(p_0) = \overrightarrow{W}_{T_l} \bullet \mathbb{V}_{T_l} \end{array}\right. \tag{21}$$

By plugging the above formula (21) in (14) and (15), we can write the matrix representation of surface gradient and divergence. For a given vector field $\mathbb{V} = (\mathbb{V}(p_1), \cdots, \mathbb{V}(p_N))^t$ and a given function $f = (f(p_1), \cdots, f(p_N))^t$ on the triangulated surface $M = \{P = \{p_i\}_{i=1}^N, T = \{T_l\}_{l=1}^L\}$, the sparse differentiation matrix $\overrightarrow{W}$ is given as follows:

$$\left\{\begin{array}{l} \overrightarrow{W}(p_i,p_j) = 0 \ \text{ if } p_i,\, p_j \text{ are not two vertex of the same triangle} \\ \overrightarrow{W}(p_i,p_i) = \frac{1}{\sum_l Area(T_l)} \sum_l Area(T_l) \overrightarrow{w}_{T_l}^{p_i}, \quad i = 1, \cdots, N \\ \overrightarrow{W}(p_i,p_j) = \frac{1}{\sum_l Area(T_l)} (Area(T_{l_1}) \overrightarrow{w}_{T_{l_1}}^{p_j} + Area(T_{l_2}) \overrightarrow{w}_{T_{l_2}}^{p_j}) \ , \\ \qquad\qquad\quad \text{if } T_{l_1} \text{ and } T_{l_2} \text{ are two common triangles of } p_i \text{ and } p_j \end{array}\right. \tag{22}$$

where l goes through the first ring of p_i. Then we have:

$$\left\{\begin{array}{l} \nabla_M f = \overrightarrow{W} f \\ \mathrm{div}_M \mathbb{V} = \overrightarrow{W} \bullet \mathbb{V} \end{array}\right. \tag{23}$$

Remark 2. *To the best of our knowledge, we are the first to write down surface gradient and divergence as matrix product in the above compact form. The biggest advantage of this sparse matrix representation is to speed up the computation. In this paper, our main concern is solving the total variation related imaging models. To solve total variational related problems, iterative methods are commonly used. With our above surface differential operator matrix representation, we only need to compute a series of sparse matrix products instead of computing gradient and divergence directly by their definition in each iteration. It is clear that we can save much more time in this way.*

3. The Total Variation and Image Processing Models on Surfaces

In variational models of image processing on the plane, total variation plays an important role as a regularizing term. One can expect that the analogue of total variation on surfaces and similar variational models should also be useful in image processing on surfaces. In this section, we first describe the generalization of the total variation concept on surfaces, and then we prove it has similar boundary perimeter formula and co-area formula as on plane cases. After these preparations, we can consider the analogous variational models on surfaces. In particular, we explain the generalization of ROF denoising and CV segmentation as two examples. One can use the same technique to generalize other plane image models to surface image models.

3.1. The total variation on surfaces

For a given surface M, denote the tangent bundle of M by TM and write the set of C^1 sections of TM, i.e. the set of C^1 tangent vector fields on M, by $\Gamma(TM)$. For any function $\varphi \in L^1(M)$, the total variation (TV) of φ is given by [3]:

$$TV(\varphi) = \sup_{\mathbb{V}\in\Gamma(TM),|\mathbb{V}|\leqslant 1} \int_M \varphi \mathrm{div}_M \mathbb{V} \mathrm{d}s \tag{24}$$

Let's write $BV(M)$ for all functions in $L^1(M)$ with finite TVs. If φ is a C^1 function, then $TV(\varphi) = \int_M |\nabla_M \varphi| \mathrm{d}s$. Therefore, we also use $\int_M |\nabla_M \varphi| \mathrm{d}s$ to denote the total variation of φ for convenience.

The importance of the total variation in imaging on 2D planes is that: 1. TV does not penalize edges of image due to the co-areaformula; 2. TV can also control the geometry of boundary because of the boundary perimeter formula. The rigorous proof of these two formulas can be found in [24, 25]. With the similar proof as in Euclidean cases, we can still have the analogue of these two formulas on surfaces. This tells us that it is reasonable to consider the total variation when we study image processing on surfaces. Moreover, we can similarly adapt other properties of total variation in Euclidean spaces to surfaces by using differential geometry techniques and functional analysis on manifolds.

Let $E \subset M$ be a measurable subset in M and χ_E be its characteristic function. We can similarly define the perimeter $Per(E)$ of E by $TV(\chi_E)$. Since the definition of the total variation on surfaces is a natural extension from the Euclidean case, we can similarly prove the following theorem by combining with differential geometry:

Theorem 1 (boundary perimeter formula). *Let E be a connected subset in M with C^2 boundary, then*

$$Per(E) = \int_M |\nabla_M \chi_E| \mathrm{d}s = length(\partial E) \tag{25}$$

[proof]: Remember

$$Per(E) = TV(\chi_E) = \sup_{\mathbb{V}\in\Gamma(TM), |\mathbb{V}|\leqslant 1} \int_M \chi_E \mathrm{div}_M \mathbb{V} \mathrm{d}s$$

Let $\overrightarrow{n}$ be the unit normal vector of ∂E. Then, for any $\mathbb{V} \in \Gamma(TM)$ with $|\mathbb{V}| \leqslant 1$, we have

$$\begin{aligned} |\int_M \chi_E \mathrm{div}_M \mathbb{V} \mathrm{d}s| = |\int_E \mathrm{div}_M \mathbb{V} \mathrm{d}s| &= |\int_{\partial E} \mathbb{V} \cdot \overrightarrow{n} \mathrm{d}l| \leqslant \int_{\partial E} 1 \mathrm{d}l = \mathrm{length}(\partial E) \\ \Longrightarrow Per(E) &\leqslant \mathrm{length}(\partial E). \end{aligned}$$

On the other hand, since ∂E is C^2 smooth, one can easily construct a tangent vector field $\overrightarrow{V_0} \in \Gamma(TM)$, such that $\overrightarrow{V_0}|_{\partial E} = \overrightarrow{n}$. Then,

$$\begin{aligned} \int_M \chi_E \mathrm{div}_M \overrightarrow{V_0} \mathrm{d}s = \int_E \mathrm{div}_M \overrightarrow{V_0} \mathrm{d}s &= \int_{\partial E} \overrightarrow{V_0} \cdot \overrightarrow{n} \mathrm{d}l = \int_{\partial E} 1 \mathrm{d}l = \mathrm{length}(\partial E) \\ \Longrightarrow Per(E) &\geqslant \mathrm{length}(\partial E) \end{aligned}$$

Therefore, $$Per(E) = \mathrm{length}(\partial E)$$ □

Furthermore, we also have the analogue of the co-area formula. To prove co-area formula for bounded variation functions on surfaces, we need to use its smooth version as follows. It is a standard result in differential geometry. The main idea of the proof is simply change of variables [14].

Theorem 2 (Smooth Co-area formula). *Given $\varphi \in C^\infty(M)$, we write $E_t = \{p \in M |\ \varphi(p) > t\ \}$. Then*

$$TV(\varphi) = \int_M |\nabla_M \varphi| \mathrm{d}s = \int_{-\infty}^{+\infty} Per(E_t) \mathrm{d}t \tag{26}$$

Now, we prove the co-area formula on surfaces. The idea of the proof is similar to Euclidean case in [24]. We prove it as follows by using the result of Theorem.2

Theorem 3 (Co-area formula). *Given $\varphi \in TV(M)$, we write $E_t = \{p \in M|\ \varphi(p) > t\ \}$. Then*

$$TV(\varphi) = \int_M |\nabla_M \varphi| \mathrm{d}s = \int_{-\infty}^{+\infty} Per(E_t) \mathrm{d}t \tag{27}$$

[Proof]: For any real number t, we define a L^1 measurable function b_t on M by:

$$b_t(p) = \begin{cases} \chi_{E_t}(p), & \text{if } t \geqslant 0 \\ -\chi_{E_t^c}(p) = \chi_{E_t}(p) - 1, & \text{if } t < 0 \end{cases}$$

Given an arbitrary point $p \in M$,

$$\int_{-\infty}^{+\infty} b_t(p) \mathrm{d}t = \begin{cases} \int_0^{\varphi(p)} \chi_{E_t}(p) \mathrm{d}t = \int_0^{\varphi(p)} 1 \mathrm{d}t = \varphi(p), & \text{if } \varphi(p) \geqslant 0 \\ -\int_{\varphi(p)}^0 \chi_{E_t^c}(p) \mathrm{d}t = -\int_{\varphi(p)}^0 1 \mathrm{d}t = \varphi(p), & \text{if } \varphi(p) < 0 \end{cases}$$

Hence, for any $\mathbb{V} \in \Gamma(TM)$ with $|\mathbb{V}| \leqslant 1$, by Fubini's theorem

$$\begin{aligned} \int_M \varphi \mathrm{div}_M \mathbb{V} \mathrm{d}s &= \int_M \left(\int_{-\infty}^{+\infty} b_t \mathrm{d}t \right) \mathrm{div}_M \mathbb{V} \mathrm{d}s \\ &= \int_{-\infty}^{+\infty} \left(\int_M b_t \mathrm{div}_M \mathbb{V} \mathrm{d}s \right) \mathrm{d}t \\ &= \int_{-\infty}^{+\infty} \left(\int_M \chi_{E_t} \mathrm{div}_M \mathbb{V} \mathrm{d}s \right) \mathrm{d}t \\ &\leqslant \underline{\int}_{-\infty}^{+\infty} Per(E_t) \mathrm{d}t \end{aligned}$$

where $\underline{\int}$ and $\overline{\int}$ denote lower and upper Lebesgue integrals respectively. Then we have:

$$TV(\varphi) \leqslant \underline{\int}_{-\infty}^{+\infty} Per(E_t) \mathrm{d}t.$$

On the other hand, one can find a sequence $\{\varphi_k\} \subset C^\infty(M)$, such that:

$$\begin{aligned} \lim_{k \to \infty} \int_M |\varphi - \varphi_k| \ \mathrm{d}s &= 0 & (a) \\ \lim_{k \to \infty} \int_M |\nabla_M \varphi_k| \ \mathrm{d}s &= TV(\varphi) \end{aligned}$$

Denote $E_t^k = \{x \in M \mid \varphi_k > t\}$, then from the smooth co-area formula on surfaces, we have:

$$\int_M |\nabla_M \varphi_k| \, \mathrm{d}s = \int_{-\infty}^{+\infty} Per(E_t^k)\mathrm{d}t, \quad \text{for each } k$$

From (a), it is clear that there is a zero measure subset $N \subset \mathbb{R}$, such that for any $t \in \mathbb{R} - N$,

$$\lim_{k\to\infty} \int_M |\chi_{E_t} - \chi_{E_t^k}| \, \mathrm{d}s = 0 \qquad (b)$$

Given $t \in \mathbb{R} - N$, if $TV(\chi_{E_t}) < \infty$, (b) implies

$$\lim_{k\to\infty} TV(\chi_{E_t^k}) = TV(\chi_{E_t})$$

Thus for any $\epsilon > 0$, there is a integer k_0, such that for $k \geqslant k_0$,

$$TV(\chi_{E_t}) \leqslant TV(\chi_{E_t^k}) + \epsilon$$

This implies:

$$Per(E_t) = TV(\chi_{E_t}) \leqslant \lim_{k\to\infty} \inf TV(\chi_{E_t^k}) \qquad (c)$$

If $TV(\chi_{E_t}) = \infty$, (c) is also true. Now by Fatou's lemma, we have:

$$\begin{aligned} \overline{\int_{-\infty}^{+\infty}} Per(E_t)\mathrm{d}t &\leqslant \int_{-\infty}^{+\infty} \lim_{k\to\infty} \inf TV(\chi_{E_t^k})\mathrm{d}t \\ &\leqslant \lim_{k\to\infty} \inf \int_{-\infty}^{+\infty} TV(\chi_{E_t^k})\mathrm{d}t \\ &= \lim_{k\to\infty} \inf TV(\varphi_k) = TV(\varphi) \end{aligned}$$

— To conclude, we have:

$$TV(\varphi) \leqslant \underline{\int_{-\infty}^{+\infty}} Per(E_t)\mathrm{d}t \leqslant \overline{\int_{-\infty}^{+\infty}} Per(E_t)\mathrm{d}t \leqslant TV(\varphi)$$

Therefore: $TV(\varphi) = \int_{-\infty}^{+\infty} Per(E_t)\mathrm{d}t$ □

In the following two subsections, as two examples, we will generalize ROF denoising and CV segmentation to show how to adapt variational models on Euclidean domains to variational models on surfaces by differential geometry techniques.

3.2. Variational models on surfaces

Similar to variational problems in the Euclidean space $\mathbb{R}^n$, a general setting of variational problems on a surface M can be written as:

$$\min_{\varphi \in \mathcal{S}} \mathcal{J}(\varphi) + \mathcal{H}(\varphi) \tag{28}$$

where $\mathcal{S}$ is certain function space on M, $\mathcal{J}$ and $\mathcal{H}$ are two convex functions on $\mathcal{S}$. In particular, let $\mathcal{S} = BV(M)$ and $\mathcal{J}(\varphi) = TV(\varphi)$ as we discussed in Section 3.1, the general variational problem (28) becomes the total variation related problems on the surface M. More specifically, we list the surface analogous forms of several popular total variational models as follows:

A. *The ROF model on surfaces*

The Rudin-Osher-Fatemi (ROF) image denoising model was first introduced by Rudin et al.[39] in plane image cases. Similarly, let $I : M \to \mathbb{R}$ be an image on a surface M. Let $\mathcal{J}(\varphi) = \int_M |\nabla_M \varphi| \mathrm{d}s, \mathcal{H}(\varphi) = \frac{\mu}{2} \int_M (\varphi - I)^2 \mathrm{d}s$, the analogous ROF image denoising model on the surface M can be represented as follows:

$$\min_{\varphi \in BV(M)} E_1(\varphi) = \int_M |\nabla_M \varphi| \mathrm{d}s + \frac{\mu}{2} \int_M (\varphi - I)^2 \mathrm{d}s \tag{29}$$

More general, let $\mathcal{H}(\varphi) = \frac{\mu}{2} \int_M (K\varphi - I)^2 \mathrm{d}s$ the analogue of the total variational image deblurring model can be written as:

$$\min_{\varphi \in BV(M)} E_2(\varphi) = \int_M |\nabla_M \varphi| \mathrm{d}s + \frac{\mu}{2} \int_M (K\varphi - I)^2 \mathrm{d}s \tag{30}$$

where K is a linear blurring kernel operator on M.

B. *The total variation inpainting model*

The total variation inpainting model was first introduced by Chan and Shen [11]. Similarly, assume $I : M \to \mathbb{R}$ is an image on the surface M. Let $D \subset M$ be the inpainting domain of I and $\mathcal{H}(\varphi) = \int_{M-D} (\varphi - I)^2 \mathrm{d}s$. The analogous total variational inpainting model on surfaces can be written as the following:

$$\min_{\varphi \in BV(M)} E_3(\varphi) = \int_M |\nabla_M \varphi| \mathrm{d}s + \frac{\mu}{2} \int_{M-D} (\varphi - I)^2 \mathrm{d}s \tag{31}$$

C. *CV segmentation and its convexified version*

The CV segmentation model was first introduced by Chan and Vese [12] for segmentation of images in the Euclidean space. For the surface case, suppose $I : M \to \mathbb{R}$ is an image on surface M. We also represent a closed curve C on M

as the zero level let of a function $\varphi : M \to \mathbb{R}$. The CV segmentation model on M can be given by:

$$\min_{\varphi,c_1,c_2} \int_M |\nabla_M H(\varphi)|\mathrm{d}s + \mu \int_M (c_1 - I)^2 H(\varphi)\mathrm{d}s + \mu \int_M (c_2 - I)^2 (1 - H(\varphi))\mathrm{d}s \quad (32)$$

where H denotes the one dimensional Heaviside function.

However, the energy of CV model is not convex, it might get "stuck" at certain local minima. Chan et al. [10] propose another convexified CV(CCV) segmentation model based on a convex energy. It can be adapted to a segmentation model on surfaces. Namely, fix $\mu \in (0, 1)$ and let $\Omega^+(\varphi^k) = \{p \in M \mid \varphi^k(p) \geqslant \mu\}$ and $\Omega^-(\varphi^k) = \{p \in M \mid \varphi^k(p) < \mu\}$, the whole procedure of optimizing CCV segmentation would be iterating the following two steps until the steady state:

1. Solve $\varphi^{k+1} = arg \min\limits_{0 \leqslant \varphi \leqslant 1} \int_M |\nabla_M \varphi| + \mu \int_M \varphi((c_1^k - I)^2 - (c_2^k - I)^2)\mathrm{d}s$
2. Update $c_1^{k+1} = \int_{\Omega^+(\varphi^{k+1})} I\mathrm{d}s$, $c_2^{k+1} = \int_{\Omega^-(\varphi^{k+1})} I\mathrm{d}s$

Thanks to differential geometry, we can easily adapt the total variational image models to surface by using differential geometry terminology. With similar techniques, many other popular variational PDE models in Euclidean space can be generalized on surfaces.

4. Numerical Algorithms for Total Variation Related Problems on Surfaces

To solve the above minimization problems, a direct method could be used is gradient descent method to find the minimizer. However, it has its own limitation of computation speed. As an advantage of the intrinsic method, it is easy to adapt popular fast algorithms to the above total variation related problems on surfaces. As examples, we will focus on solving the ROF denoising model and the CCV segmentation models on surfaces by adapting two fast algorithms, namely the split Bregman iteration method and Chambolle's dual projection method. Similar approaches can be used to solve other relevant models on surfaces.

4.1. Primal approaches: Split Bregmen iterations

Bregman iteration is first introduced by S. Osher et al.[38]. Later, Tom Goldstein et al. [27, 26] introduce the split Bregman method to compute ROF and global convex segmentation problems in plane image cases. The convergence analysis of this algorithm is given by J.F. Cai et al. in [8]. This algorithm is much faster than gradient descent. Here we can adapt their algorithms to solve the total variation related problems on surfaces as follows.

We consider a general total variation related optimization problem on surfaces:

$$\min_{\varphi} \int_{M} |\nabla_M \varphi| \mathrm{d}s + \mathcal{H}(\varphi) \tag{33}$$

where $\mathcal{H}(\cdot)$ is a convex function.

Let $\Gamma(TM)$ be the linear space of all tangent vector fields on M. We also introduce the auxiliary variable $\mathbb{V} \in \Gamma(TM)$, and consider the following equivalent optimization problem:

$$\min_{\varphi, \mathbb{V} \in \Gamma(TM)} ||\mathbb{V}||_1 + \mathcal{H}(\varphi) \quad \text{subject to} \quad \mathbb{V} = \nabla_M \varphi \tag{34}$$

where $||\mathbb{V}||_1$ is defined in (7). The corresponding unconstrained problem would be:

$$(\varphi^*, \mathbb{V}^*) = arg \min_{\varphi, \mathbb{V} \in \Gamma(TM)} ||\mathbb{V}||_1 + \mathcal{H}(\varphi) + \frac{\lambda}{2} ||\mathbb{V} - \nabla_M \varphi||_2^2 \tag{35}$$

Then, we can apply the Bregman iteration on the above problem, namely, we should solve a sequence of the following problems:

$$\begin{aligned} (\varphi^k, \mathbb{V}^k) &= arg \min_{\varphi, \mathbb{V} \in \Gamma(TM)} ||\mathbb{V}||_1 + \mathcal{H}(\varphi) + \frac{\lambda}{2} ||\mathbb{V} - \nabla_M \varphi - \overrightarrow{b}^k||_2^2 &\quad (36) \\ \overrightarrow{b}^{k+1} &= \overrightarrow{b}^k + \nabla_M \varphi^k - \mathbb{V}^k &\quad (37) \end{aligned}$$

To solve (36), we can iteratively minimize with respect to φ and $\mathbb{V}$ separately:

$$\begin{aligned} \varphi^{k+1} &= arg \min_{\varphi} \mathcal{H}(\varphi) + \frac{\lambda}{2} ||\mathbb{V}^k - \nabla_M \varphi - \overrightarrow{b}^k||_2^2 &\quad (38) \\ \mathbb{V}^{k+1} &= arg \min_{\mathbb{V} \in \Gamma(TM)} ||\mathbb{V}||_1 + \frac{\lambda}{2} ||\mathbb{V} - \nabla_M \varphi^{k+1} - \overrightarrow{b}^k||_2^2 &\quad (39) \end{aligned}$$

For (39), the solution is also similar to plane image cases, which can be obtained by the following shrinkage:

$$\mathbb{V}^{k+1} = \max\{|\nabla_M \varphi^{k+1} + \overrightarrow{b}^k| - 1/\lambda, 0\} \frac{\nabla_M \varphi^{k+1} + \overrightarrow{b}^k}{|\nabla_M \varphi^{k+1} + \overrightarrow{b}^k|} \tag{40}$$

To summarize, the whole procedure of using split Bregman iterations for the minimization problem (33) on the surface M is the following:

1. Let $\mathbb{V}^0 = \overrightarrow{b}^0 = 0$, Do

2. Update $\varphi^{k+1} = arg\min_{\varphi} \mathcal{H}(\varphi) + \frac{\lambda}{2}||\mathbb{V}^k - \nabla_M\varphi - \overrightarrow{b}^k||_2^2$;
3. Update $\mathbb{V}^{k+1} = \max\{|\nabla_M\varphi^{k+1} + \overrightarrow{b}^k| - 1/\lambda, 0\}\frac{\nabla_M\varphi^{k+1}+\overrightarrow{b}^k}{|\nabla_M\varphi^{k+1}+\overrightarrow{b}^k|}$;
4. Update $\overrightarrow{b}^{k+1} = \overrightarrow{b}^k + \nabla_M\varphi^{k+1} - \mathbb{V}^{k+1}$;
5. while ("not converge")

Fact 1. *If the initial auxiliary variables* $\overrightarrow{b}^0$,$\mathbb{V}^0$ *are two tangent vector fields on* M*, then each* $\overrightarrow{b}^k$,$\mathbb{V}^k$ *will also be tangent fields on* M*.*

[Proof]: By the definition of step 3 and 4 in above algorithm, and using induction on k, the fact is obviously true. □

When we implement the above algorithms, the surface we consider is an embedding surface in $\mathbb{R}^3$, thus a tangent vector on the surface can also be viewed as a vector in $\mathbb{R}^3$. By Fact 1, if the initial data $\overrightarrow{b}^0$,$\mathbb{V}^0$ are two tangent vector fields on the surface, the results of each iteration are automatically two tangent vector fields of the given surface, even if we view the tangent vector field as a vector field in $\mathbb{R}^3$.

A. *Split Bregman iteration for ROF deoising model on surfaces.*

In ROF denoising model (31), $\mathcal{H}(\varphi) = \frac{\mu}{2}||\varphi - I||_2^2$. In this case, the solution of the minimization problem (38) should satisfy:

$$(\mu\mathrm{Id} - \lambda\triangle_M)\varphi^{k+1} = \mu I + \lambda\ \mathrm{div}_M(\overrightarrow{b}^k - \mathbb{V}^k) \tag{41}$$

Therefore, the split Bregman iteration for ROF denoising model (31) would be given by:

1. Let $\mathbb{V}^0 = \overrightarrow{b}^0 = 0$, Do
2. Solve $(\mu\mathrm{Id} - \lambda\triangle_M)\varphi^{k+1} = \mu I + \lambda\ \mathrm{div}_M(\overrightarrow{b}^k - \mathbb{V}^k)$;
3. Update $\mathbb{V}^{k+1} = \max\{|\nabla_M\varphi^{k+1} + \overrightarrow{b}^k| - 1/\lambda, 0\}\frac{\nabla_M\varphi^{k+1}+\overrightarrow{b}^k}{|\nabla_M\varphi^{k+1}+\overrightarrow{b}^k|}$;
4. Update $\overrightarrow{b}^{k+1} = \overrightarrow{b}^k + \nabla_M\varphi^{k+1} - \mathbb{V}^{k+1}$;
5. while ("not converge")

B. *Split Bregman iterations for CCV segmentation model on surfaces*

The key step in CCV segmentation model is solving

$$\varphi^{k+1} = arg\min_{0\leqslant\varphi\leqslant 1}\int_M |\nabla_M\varphi| + \mu\int_M \varphi r^k \mathrm{d}s \tag{42}$$

where $r^k = (c_1^k - I)^2 - (c_2^k - I)^2$. In this case, we have $\mathcal{H}(\varphi) = \mu \int_M \varphi r^k \mathrm{d}s$. The minimization problem (38) becomes:

$$\varphi^{k+1} = arg \min_{0 \leqslant \varphi \leqslant 1} \frac{\lambda}{2} ||\mathbb{V}^k - \nabla_M \varphi - \overrightarrow{b}^k||_2^2 + \mu \int_M \varphi r^k \mathrm{d}s \tag{43}$$

Since the above minimization is a quadratic problem with constraint $0 \leqslant \varphi \leqslant 1$, its solution can be obtained by:

$$\begin{aligned} \text{solve:} \quad \triangle_M \varphi^{k+1} &= \frac{\mu}{\lambda} r^k + \mathrm{div}_M(\mathbb{V}^k - \overrightarrow{b}^k) \\ \text{update:} \quad \varphi^{k+1}(p_i) &\longleftarrow \min\{\max\{\varphi^{k+1}(p_i), 0\}, 1\} \end{aligned} \tag{44}$$

Therefore, the split Bregman iteration for CCV segmentation model would be given by:

1. Let $\mathbb{V}^0 = \overrightarrow{b}^0 = 0$, Do
2. Update $r^k = (c_1^k - I)^2 - (c_2^k - I)^2$;
3. Solve $\triangle_M \varphi^{k+1} = \frac{\mu}{\lambda} r^k + \mathrm{div}_M(\mathbb{V}^k - \overrightarrow{b}^k)$,
   $\varphi^{k+1}(p_i) \longleftarrow \min\{\max\{\varphi^{k+1}(p_i), 0\}, 1\}$;
4. Update $\mathbb{V}^{k+1} = \max\{|\nabla_M \varphi^{k+1} + \overrightarrow{b}^k| - 1/\lambda, 0\} \frac{\nabla_M \varphi^{k+1} + \overrightarrow{b}^k}{|\nabla_M \varphi^{k+1} + \overrightarrow{b}^k|}$;
5. Update $\overrightarrow{b}^{k+1} = \overrightarrow{b}^k + \nabla_M \varphi^{k+1} - \mathbb{V}^{k+1}$;
6. Update $c_1^{k+1} = \int\limits_{\Omega^+(\varphi^{k+1})} I \mathrm{d}s$, $c_2^{k+1} = \int\limits_{\Omega^-(\varphi^{k+1})} I \mathrm{d}s$;
7. while ("not converge")

4.2. Dual approaches: Chambolle's projection methods

The discussion based on the variational model (33) with split Bregman iteration method, can be viewed as the primal approach to solve the total variation related problems on surfaces. Meanwhile, based on the definition of the total variation, there has been increasing interests on dual approaches. One famous dual algorithm is Chambolle's projection method of ROF denoising model [9]. It offers us a fast and easy-coding algorithm to solve ROF denoising model. Later, X. Bresson et al [6] propose an algorithm based on Chambolle's projection method to solve CCV model for plane image problems. Here, we can similarly apply the Chambolle's projection methods to solve the total variation related optimization problems on surfaces. Remembering the definition of the total variation on surfaces in (24), we consider the following variational problem:

$$\min_{\varphi} \sup_{\mathbb{V} \in \Gamma(TM), |\mathbb{V}| \leqslant 1} \int_M \varphi \mathrm{div}_M \mathbb{V} \mathrm{d}s + \mathcal{H}(\varphi) \tag{45}$$

By the min-max theorem in optimization theory [21], we can interchange the min and max, to obtain the following equivalent optimization problem:

$$\max_{\mathbb{V}\in\Gamma(TM),|\mathbb{V}|\leqslant 1}\min_{\varphi}\int_M \varphi \mathrm{div}_M \mathbb{V} \mathrm{d}s + \mathcal{H}(\varphi) \tag{46}$$

A. *Dual method for ROF denoising model on surfaces*

In ROF denoising model (31), $\mathcal{H}(\varphi) = \frac{\mu}{2}||\varphi - I||_2^2$. In this case, we need to consider the following problem:

$$\max_{\mathbb{V}\in\Gamma(TM),|\mathbb{V}|\leqslant 1}\min_{\varphi}\int_M \varphi \mathrm{div}_M \mathbb{V} \mathrm{d}s + \frac{\mu}{2}||\varphi - I||_2^2 \tag{47}$$

The solution of the inner minimization problem can be solved exactly as $\varphi = I - \frac{1}{\mu}\mathrm{div}_M \mathbb{V}$. Plug in this back to the above problem, we have the following maximization problem:

$$\begin{aligned}
& arg \max_{\mathbb{V}\in\Gamma(TM),|\mathbb{V}|\leqslant 1}\int_M (I - \frac{1}{\mu}\mathrm{div}_M \mathbb{V})\mathrm{div}_M \mathbb{V}\mathrm{d}s + \frac{\mu}{2}||\frac{1}{\mu}\mathrm{div}_M \mathbb{V}||_2^2 \\
= \ & arg \max_{\mathbb{V}\in\Gamma(TM),|\mathbb{V}|\leqslant 1}\frac{\mu}{2}(||I||_2^2 - ||\frac{1}{\mu}\mathrm{div}_M \mathbb{V} - I||_2^2) \\
= \ & arg \min_{\mathbb{V}\in\Gamma(TM),|\mathbb{V}|\leqslant 1}||\frac{1}{\mu}\mathrm{div}_M \mathbb{V} - I||_2^2
\end{aligned} \tag{48}$$

As indicated in Chambolle's method [9], we can also solve the last minimization problem by the iterative method as follows:

$$\mathbb{V}^{n+1} = \frac{\mathbb{V}^n + \tau\nabla_M(\mathrm{div}_M \mathbb{V}^n - \mu I)}{1 + \tau|\nabla_M(\mathrm{div}_M \mathbb{V}^n - \mu I)|} \tag{49}$$

The convergence analysis in Euclidean cases can be easily adapted to surface cases to prove the convergence.

B. *Dual method for CCV segmentation model on surfaces*

The key step in CCV segmentation model is solving

$$\min_{0\leqslant\varphi\leqslant 1} TV(\varphi) + \mu\int_M \varphi r^k \mathrm{d}s \tag{50}$$

where $r^k = (c_1^k - I)^2 - (c_2^k - I)^2$. It has the same set of minimizers as the following unconstrained problem [10]:

$$\min_{\varphi} TV(\varphi) + \mu\int_M (\varphi r^k + \alpha\nu(\varphi))\mathrm{d}s \tag{51}$$

where $\nu(\xi) = \max\{0, 2|\xi - 1/2| - 1\}$, provided that $\alpha > \frac{\mu}{2}||r^k(x)||_{L^\infty}$. As the algorithms proposed in [1, 6], we can similarly consider convex regularization of the above minimization problem on surfaces as follows:

$$\min_{\varphi,v} TV(\varphi) + \frac{\theta}{2}||\varphi - v||_2^2 + \mu \int_M (vr^k + \alpha\nu(v))\mathrm{d}s \tag{52}$$

whose solution can be approached by iteratively updating φ, v by the following two steps:

$$\varphi^{l+1} = arg \min_{\varphi} TV(\varphi) + \frac{\theta}{2}||\varphi - v^l||_2^2 \tag{53}$$

$$v^{l+1} = arg \min_{v} \frac{\theta}{2}||\varphi^{l+1} - v||_2^2 + \mu \int_M (vr^k + \alpha\nu(v))\mathrm{d}s \tag{54}$$

By the dual algorithm of ROF model, the minimizer of (53) can be obtained by $\varphi^{l+1} = v^l - \frac{1}{\theta}\mathrm{div}_M\mathbb{V}$, where $\mathbb{V}$ can be iteratively solved by

$$\mathbb{V}^{n+1} = \frac{\mathbb{V}^n + \tau\nabla_M(\mathrm{div}_M\mathbb{V}^n - \theta v^l)}{1 + \tau|\nabla_M(\mathrm{div}_M\mathbb{V}^n - \theta v^l)|} \tag{55}$$

and the solution of (54) is given by $v^{l+1} = min\{max\{\varphi^{l+1} - \frac{\mu}{\theta}r^k, 0\}, 1\}$. All convergence proofs of this algorithm on surface optimization problem (50) can be naturally adapted from the proofs in Euclidean cases in [6]. To conclude, the algorithm of dual method to solve CCV segmentation model on surfaces is given as follows:

1. Let $v^0 = 0, \mathbb{V}^0 = 0$, Do
2. Update $r^k = (c_1^k - I)^2 - (c_2^k - I)^2$;
3. Do
4. Do $\mathbb{V}^{n+1} = \frac{\mathbb{V}^n + \tau\nabla_M(\mathrm{div}_M\mathbb{V}^n - \theta v^l)}{1+\tau|\nabla_M(\mathrm{div}_M\mathbb{V}^n - \theta v^l)|}$ while $(|\mathbb{V}^{n+1} - \mathbb{V}^n| > \epsilon)$
5. Update $\varphi^{l+1} = v^l - \frac{1}{\theta}\mathrm{div}_M\mathbb{V}^{n+1}$;
6. Update $v^{l+1} = min\{max\{\varphi^{l+1} - \frac{\mu}{\theta}r^k, 0\}, 1\}$
7. while $(\max\{|\varphi^{l+1} - \varphi^l|, |v^{l+1} - v^l|\} > \epsilon)$
8. Update $c_1^{k+1} = \int_{\Omega^+(\varphi^{k+1})} I\mathrm{d}s$, $c_2^{k+1} = \int_{\Omega^-(\varphi^{k+1})} I\mathrm{d}s$;
9. while ("not converge")

To summarize, we want to point out that the successful generalization of the image models and their related algorithms from Euclidean cases to surface cases is because of differential geometry. Due to the power of differential geometry, a natural extension of Euclidean geometry, we can generalize the concept of the total variation on surfaces, then ROF denoising model and CCV segmentation model and their related algorithms are adapted on surfaces as examples. Moreover, one can also prove similar convergence results as Euclidean cases. With the same technique, the generalization of fast algorithms is not necessarily limited to split Bregman iteration and dual projection method, one can similarly generalize other fast algorithms such as primal-dual methods [43, 23] and so on.

4.3. Implementation

So far, we extend all formulas on surfaces. It is easy to observe that each abstract formula is quite consistent with plane image cases due to differential geometry terminologies. At the first glance, the only difference is that we replace all Euclidean gradient, divergence, Laplace operators and Euclidean integrals by their corresponding surface forms. However, since the surface metric has been involved in the above surface differential operators and surface integrals, the mathematical meaning of each term is quite different and also numerical implementation is different.

A. *Surface differential operators*

As we described in section 2.2, the data structure of each surface is given by a triangle mesh $M = \{P = \{p_i\}_{i=1}^N, T = \{T_l\}_{l=1}^L\}$, where $p_i \in \mathbb{R}^3$ is the i-th vertex and T_l is the l-th triangle. Any function f defined on M can be written as $f = \{f(p_i)\}_{i=1}^N$. Since M is a embedding surface in $\mathbb{R}^3$, then any tangent vector $\mathbb{V}$ on M can be written as $\mathbb{V} = \{\mathbb{V}(p_i)\}_{i=1}^N$, where each $\mathbb{V}(p_i)$ can be viewed as a vector in $\mathbb{R}^3$. Let $\overrightarrow{W}$ be the differentiation vector matrix defined in section 2.3 associated with the triangle mesh M. Then we can easily compute the surface gradient and divergence by the matrix product as the discussion in section 2.3:

$$\nabla_M f = \overrightarrow{W} f; \quad \mathrm{div}_M \mathbb{V} = \overrightarrow{W} \bullet \mathbb{V} \tag{56}$$

Once we can compute the surface gradient and divergence, then the Chambolle's projection method to compute ROF denoising model and CCV segmentation model on surface can be easily implemented, since the algorithms of Chambolle's projection method only need surface gradient and divergence.

B. *Surface PDEs*

The next step is to implement the split Bregman iterations on surfaces. There are two PDEs related to the Laplace operator we need to solve on surfaces. One is to solve the equation (41) for ROF denoising:

$$(\mu \mathrm{Id} - \lambda \triangle_M)\varphi^{k+1} = \mu I + \lambda \ \mathrm{div}_M(\overrightarrow{b}^k - \mathbb{V}^k) \tag{57}$$

another one is the equation (44) for CCV segmentation. small

$$\triangle_M \varphi^{k+1} = \frac{\mu}{\lambda} r^k + \mathrm{div}_M(\mathbb{V}^k - \overrightarrow{b}^k) \tag{58}$$

Since above two equations are defined on a triangulated surface, we can not use the fast solver, fast fourier transform (FFT), to solve it as we deal with the same type of equations in 2D regular domain. One possible method is by using the discretization of $\triangle_M$ given by Meyer, Desbrun, Xu et al.[37, 19, 42], then use Gauss-Seidel, conjugate gradient to solve them. However, the approximation of Laplace-Beltrami operator on an arbitrary triangulated surface depends on the quality of triangle mesh. To avoid discretizing the second order differential operator, we are here proposing to use finite element methods to solve equations (41) and (44).

We choose the linear elements $\{e_i\}_{i=1}^N$ on triangle mesh $\{V = \{p_i\}_{i=1}^N, T = \{T_l\}_{l=1}^L\}$, such that $e_i(p_j) = \delta_{i,j}$ and write $S = Span_{\mathbb{R}}\{e_i\}_{i=1}^N$. Then the discrete version of the continuous variational problem of (41) is to find a $\varphi^{k+1} \in S$, such that

$$\mu \sum_l \int_{T_l} \varphi^{k+1} e_j + \lambda \sum_l \int_{T_l} \nabla_M \varphi^{k+1} \nabla_M e_j = \sum_l \int_{T_l} \Theta^k e_j, \ \forall e_j \in S. \tag{59}$$

where $\Theta^k = \mu I + \lambda \ \mathrm{div}_M(\overrightarrow{b}^k - \mathbb{V}^k)$.

If we write

$$\begin{cases} \varphi^{k+1} = \sum_i^N x_i e_i, \quad \Theta^k = \sum_i^N \theta_i e_i \\ Q = (a_{ij})_{N\times N}, a_{ij} = \sum_l \int_{T_l} \nabla_M e_i \nabla_M e_j \\ K = (b_{ij})_{N\times N}, b_{ij} = \sum_l \int_{T_l} e_i e_j \end{cases} \tag{60}$$

and if we also write $\varphi^{k+1} = (x_1, \cdots, x_N)^t$ and $\Theta^{k+1} = (\theta_1, \cdots, \theta_N)^t$ with abused notations, then to solve φ^{k+1} is equivalent to solving the following linear equations:

$$(\mu K + \lambda Q)\varphi^{k+1} = K\Theta \tag{61}$$

One fact we would like to point out here is:

Fact 2. *K is a symmetric positive definite sparse matrix and Q is a symmetric nonnegative definite sparse matrix.*

[Proof]: Symmetry of Q, K is easy to see. For any $f = (f_1, \cdots, f_N)^t, g = (g_1, \cdots, g_N)^t$, if we also write $f = \sum f_i e_i$ and $g = \sum g_i e_i$, then $fKg^t = \int_M fg$ and $fQg^t = \int_M \nabla_M f \nabla_M g$. So K is positive definite and Q is nonnegative definite. □

Therefore, when μ and λ are both positive, the matrix $(\mu K + \lambda Q)$ is a symmetric positive definite sparse matrix. The solution φ^{k+1} of (61) can be obtained by using conjugate gradient or Gauss-Seidel.

Similarly, the discrete version of the continuous variational problem of (44) is to find a $\varphi^{k+1} \in S$, such that

$$\sum_l \int_{T_l} \nabla_M \varphi^{k+1} \nabla_M e_j = -\sum_l \int_{T_l} \Gamma^k e_j, \ \forall e_j \in S. \tag{62}$$

where $\Gamma^k = \frac{\mu}{\lambda} r^k + \mathrm{div}_M(\mathbb{V}^k - \overrightarrow{b}^k)$.

If we write $\varphi^{k+1} = \sum_i^N x_i e_i, \quad \Gamma^k = \sum_i^N \gamma_i e_i$, the solution φ^{k+1} of (44) is equivalent to solving the following linear equation:

$$Q\varphi^{k+1} = -K\Gamma^k \tag{63}$$

which can be solved by the Gauss-Seidel method.

5. Experiment Results and Applications

In this section, several examples will be given to demonstrate advantages of the intrinsic method. The intrinsic method can provide us a robust and efficient method to study image problems on surfaces. It can easily handle surfaces with different complexity, different topologies. Moreover, we will further show two applications of our intrinsic method of image processing on surfaces. All algorithms are written in C++ and all experiments are ran on a PC with a 2.0GHz CPU.

5.1. Comparison with other approaches

The intrinsic method can efficiently solve variational problems directly on surfaces and does not need preprocessing. Due to the natural extension of differential operators on surfaces, the fast algorithms for variational problems in Euclidean cases can also be easily adapted on surfaces by this intrinsic method. To demonstrate these advantages of our intrinsic method, we here compare our method with level set method and conformal parametrization method. We test the CCV segmentation model on following two surfaces $M1, M2$ with characters by the intrinsic method, the level set method [29, 36] and the conformal parametrization method [33] respectively. In Figure 1, Surface $M2$ is a cortical surface in human's brain[1] and surface $M1$ is a smoothing version of surface $M2$. Both surfaces have 39994 vertices. The computation cost comparison is listed in table 2.

From Table 2, we can observe two facts as follows:

[1]Meshes are provided by the public available database ADNI at LONI

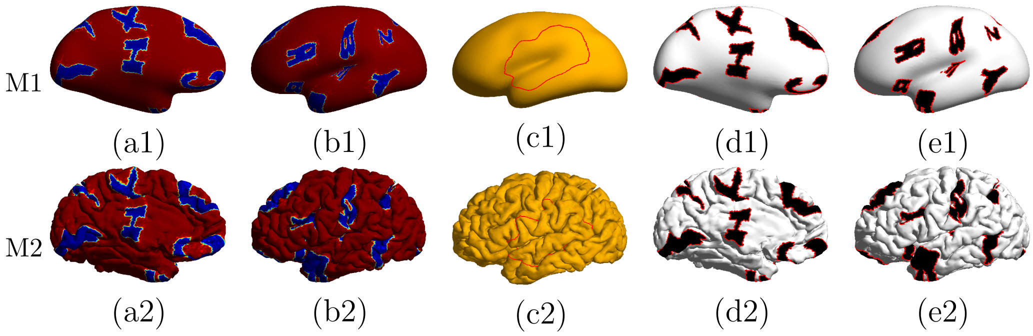

Figure 1: CCV segmentation results on two surfaces with different complexity. The first row: (a1), (b1) two views of characters image I on surface $M1$, (c1) the initial curve for CCV segmentation on $M1$, (d1), (e1) two views of the CCV segmentation results φ. The second row: (a2),(b2) two views of characters image I on surface $M2$, (c2) the initial curve for CCV segmentation on $M2$, (d2), (e2) two views of the CCV segmentation results φ.

	intrinsic method	conformal parametrization	level set
M1	CCV by split Bregman 18.61s	parametrization: 126.63s + CCV by split Bregman in 0.55s	implicit representation with $65 \times 162 \times 99$ grid points in 5.92s + CCV by gradient descent in 84.44s
M2	CCV by split Bregman 18.94s	parametrization: 602.91s + CCV by split Bregman in 0.56s	implicit representation with $143 \times 350 \times 227$ grid points in 29.55s + CCV by gradient descent in 756.4s

Table 2: The computation cost of different methods.

1. Computation cost under surface structure variance:
   For the conformal parametrization method and level set method, they both depend on the complexity of surfaces. More specifically, it needs more time to obtain the conformal parametrization if the surface geometry is farther from the sphere. Similarly, the level set method also needs more data to represent a surface with more complicated structure, which requires more time to solve variational problems. However, the computation of the intrinsic method is fast and stable under surface structure variance.
2. Adaptability of fast algorithms:
   For the conformal parametrization method, once the parametrization is obtained, one can easily transfer the surface variational problems into 2D Euclidean cases, then several fast algorithms can be also applied. For the level set method, since the surface gradient operator is computed by projection

and expression of surface divergence by level set function is very complicated, the generalization of fast algorithms, like split Bregman or Chambolle's projection method is not straightforward. Meanwhile, the data size of implicit surface representation will consume more computation cost. However, as we discussed in section 4.3, fast algorithms in Euclidean cases can be easily adapted in surface cases by the intrinsic method.

5.2. Further demonstration on high genus surfaces and open surfaces

In many fields such as computer graphics, geometry modeling, medical imaging, computational anatomy, 3D cartoon, it is also necessary to process high genus surfaces or open surfaces. Usually, to find a parametrization of a high genus surface is not so easy, one has to cut the surface into several patches [28, 35], then process these patches separately. This artificial cutting of patches and separately processing may introduce numerical inaccuracy on the cutting edges. In addition, the parametrization method and level set method have their own limitations to study open surfaces, specially open surfaces with topological nontrivial boundaries. However, the intrinsic method can easily handle high genus surfaces and open surfaces as surfaces with spherical topology.

Here, we demonstrate this advantage of the intrinsic method in several synthetic examples. In Figure 2, we take a one handled cup [2] with 25075 vertices as a ground surface and show ROF denoising results of the Lena image with Gaussian noise $\sigma = 40$. As we discussed in Section 4, the split Bregman iterations and Chambolle's dual projection method can be applied to solve ROF denoising models on surfaces. We show denoising results obtained by split Bregman and Chambolle's dual projection method respectively in Figure 2. In addition, we also apply our algorithms for the CCV segmentation model on surfaces to the same one handled cup and a torus. The segmentation results are showed in Figure 3 and Figure 4. Moreover, to show the advantage of dealing with open surfaces with the intrinsic method, we show CCV segmentation results in Figure 5 on a human hand surface [3] and Figure 6 on a half torus, which both are open surfaces. To summarize, our intrinsic method can provide a robust and efficient approach to study image problems on surfaces, whenever surfaces are closed or open, with genus zero or high genus, with simple or complicated geometric structure.

5.3. Applications

A. *Geometric processing*

[2]One handled cup is obtained from the public available database SHARP3D

[3]This model is provided by the public available database AIM@SHAPE Shape Repository

Figure 2: ROF denoising results of the Lena image I on a 25075 vertices cup surface with split Bregman iterations and Chambolle's projection method. (a) the clear lena image. (b) the noise image with Gaussian noise σ=40. (c), (d) a denoising result φ by split Bregman iterations with $\lambda = 0.05, \mu = 1000$ in 17.73 seconds and its corresponding residual $I - \varphi$. (e), (f) a denoising result φ by Chambolle's projection method with $\mu = 10$ in 35.46 seconds and its corresponding residual $I - \varphi$.

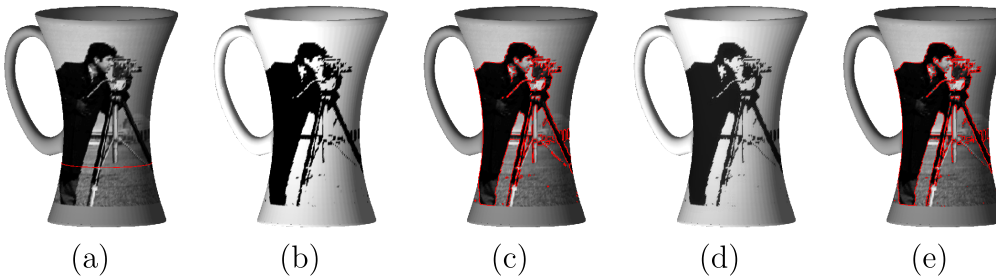

Figure 3: CCV segmentation results on a 25075 vertices cup surface with split Bregman iterations and Chambolle's projection method. (a) the cameraman image and the initial segmentation curve marked by the red contour. (b), (c) the CCV segmentation result obtained by split Bregman method with $\lambda = 8, \mu = 50$ in 14.57 seconds and the corresponding edges marked by red contours in the original image. (d), (e) the CCV segmentation result obtained by Chambolle's projection method with $\mu = 0.1, \theta = 400$ in 73.34 seconds and the corresponding edges marked by red contours in the original image.

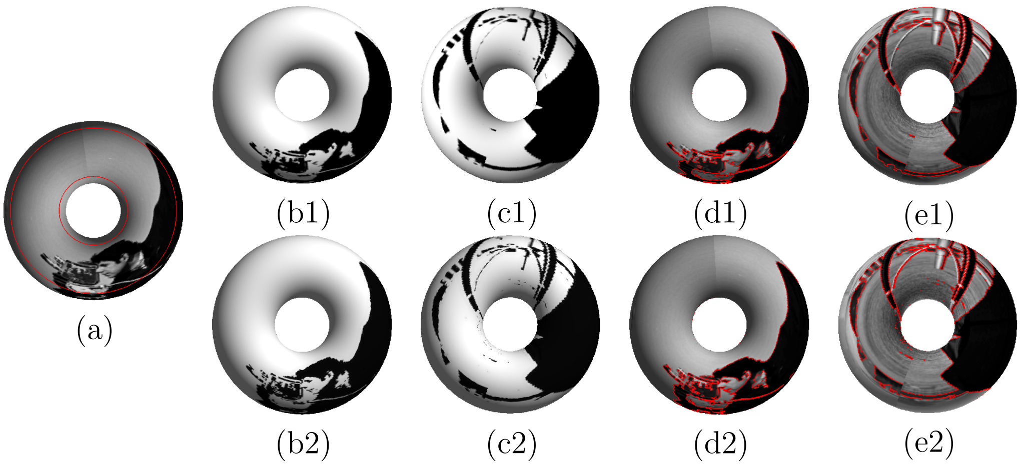

Figure 4: CCV segmentation results on a 65536 vertices torus with split Bregman iterations and Chambolle's projection method. (a) the cameraman image and the initial segmentation curve marked by the red contour. (b1), (c1), (d1), (e1) two views the CCV segmentation result obtained by split Bregman method with $\mu = 10, \lambda = 50$ in 42.95 seconds and two views of the corresponding edges marked by red contours in the original image. (b2), (c2), (d2), (e2) two views the CCV segmentation result obtained by Chambolle's projection method with $\mu = 0.1, \theta = 1000$ in 162.99 seconds and the corresponding edges marked by red contours on the original image.

An interesting application of ROF denoising is geometric processing, namely, surface denoising or geometric processing [15, 17, 18, 2, 22, 20, 33]. Given a surface $M \subset \mathbb{R}^3$, there are three coordinate functions (f_1, f_2, f_3) on M, namely we have the embedding:

$$\begin{aligned} \overrightarrow{f} = (f_1, f_2, f_3): \quad M &\longrightarrow \mathbb{R}^3 \\ p &\longmapsto (f_1(p), f_2(p), f_3(p)) \end{aligned} \tag{64}$$

It is natural to view the three coordinate functions (f_1, f_2, f_3) as three image functions on the surface M. A noisy surface is a perturbation in the geometry of the surface, namely, we can view the noisy surface $\overrightarrow{f_{noise}}$ as $\overrightarrow{f_{clear}} + \overrightarrow{noise}$ with $\overrightarrow{noise} \in \mathcal{N}(0, \sigma) \times \mathcal{N}(0, \sigma) \times \mathcal{N}(0, \sigma)$. Thus each coordinate function of the noisy surface can be viewed as a noisy image on the surface, then we can study the geometry processing via the surface coordinate functions. As an example, we naively consider surface ROF denosing model on each coordinate function as an approach to study surface denosing. Figure 7 shows two preliminary results of the surface denoising. The first row in Figure 7 is the surface denoising of a cube with Gaussian noise $\sigma = 0.1$. The edge preserving property of the total variation can be observed from the denoising result. The second row is a denoising result of a

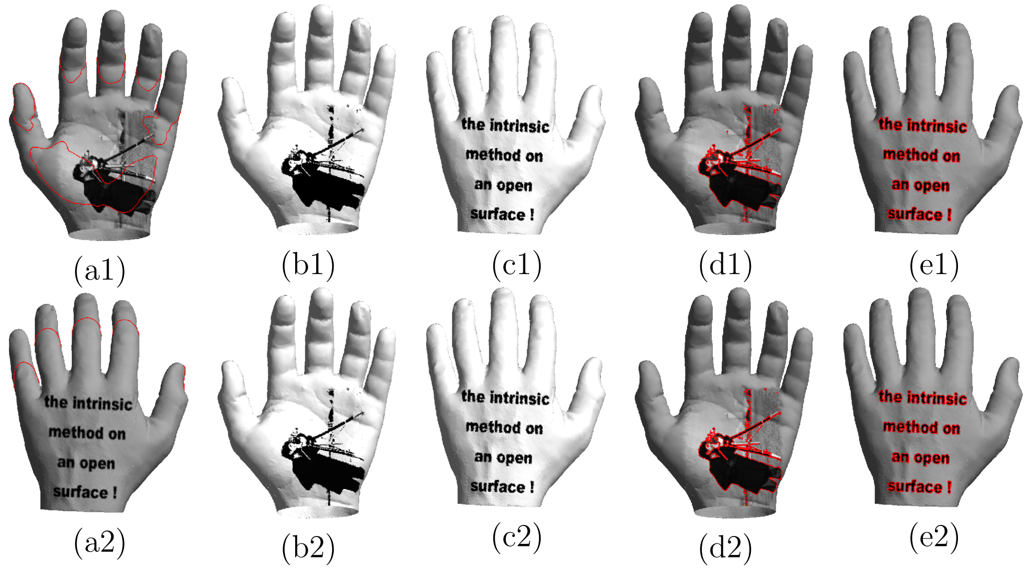

Figure 5: CCV segmentation results on a 58875 vertices open hand surface with split Bregman iterations and Chambolle's projection method. (a1), (a2) two views the image and the initial segmentation curve marked by the red contour. (b1), (c1), (d1), (e1) two views the CCV segmentation result obtained by split Bregman method with $\mu = 5, \lambda = 50$ in 29.74 seconds and two views of the corresponding edges marked by red contours in the original image. (b2), (c2), (d2), (e2) two views the CCV segmentation result obtained by Chambolle's projection method with $\mu = 0.1, \theta = 1000$ in 184.94 seconds and the corresponding edges marked by red contours on the original image.

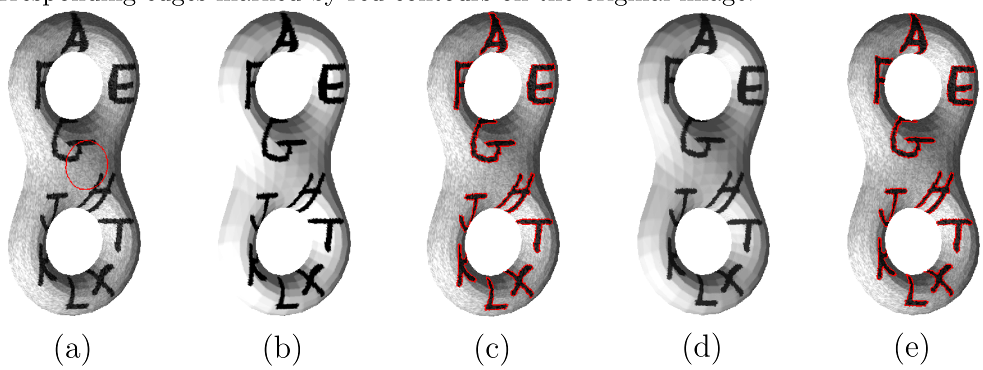

Figure 6: CCV segmentation results on a 31247 vertices half double torus with split Bregman iterations and Chambolle's projection method. (a) the characters image with Gaussian noise $\sigma = 100$ and the initial segmentation curve marked by the red contour. (b), (c) the CCV segmentation result obtained by split Bregman method with $\lambda = 100, \mu = 50$ in 21.33 seconds and the corresponding edges marked by red contours in the original image. (d), (e) the CCV segmentation result obtained by Chambolle's projection method with $\mu = 0.1, \theta = 1000$ in 108.4 seconds and the corresponding edges marked by red contours in the original image.

human's cortical surface[4].

B. *Cortical parcellation*

Image segmentation techniques are quite useful in image analysis on the 2D plane. For 3D surface analysis, image segmentation technique can also be used to detect certain special parts of the given surface. For instance, in anatomical brain structure analysis, sulci/guri detection for cortical surfaces is important [34, 40, 30]. However, in most cases, cortical surfaces have many very deep and closed folding parts. These folding parts might restrict us to easily and efficiently find parameterization or use implicit method. With our intrinsic image processing on surfaces method, we can directly process the image segmentation on cortical surfaces without any preprocessing. This will help us deal with surfaces with complex structures. For the sulci/guri detection problem, we can view the mean curvature of cortical surfaces as an image on the surfaces, which can be obtained by the algorithms given in [37], then apply CCV segmentation on mean curvature. The CCV segmentation result will give provide us a promising cortical parcellation. In Figure 8, we show the segmentation results of two type of cortical surfaces. The first row is a human's cortical surface[5] and the second row is a vervet's cortical surface[6]. Both surfaces are with deep and narrow sulcal regions.

6. Conclusions and Future Work

In this work, we use differential geometric techniques to study intrinsical image processing on surfaces. We generalize the total variation concept on surfaces and show it is also a suitable regularizing term when we study image processing on surfaces. Furthermore, we take ROF denoising model and CV segmentation model as two examples to illustrate our intrinsic method. As an advantage of the intrinsic method, we show the adaptability of fast algorithms in Euclidean spaces to the total variational related problems on surfaces by using the intrinsic method. Specifically, we implement the split Bregman method and Chambolle's dual projection method as two examples. The intrinsic method is a very general approach to study variational problems, differential equations and image processing on surfaces. This technique can be further extended to study diffusion equations, motions of curves, and other surface PDEs or variation related problems on surfaces. In the future, we will explore along this direction and demonstrate more applications of this intrinsic geometric technique.

---

[4]This model is provide by the public available database ADNI at LONI

[5]This model is obtained from the public available database ADNI at LONI

[6]This model is provided by Dr. Scott Fears

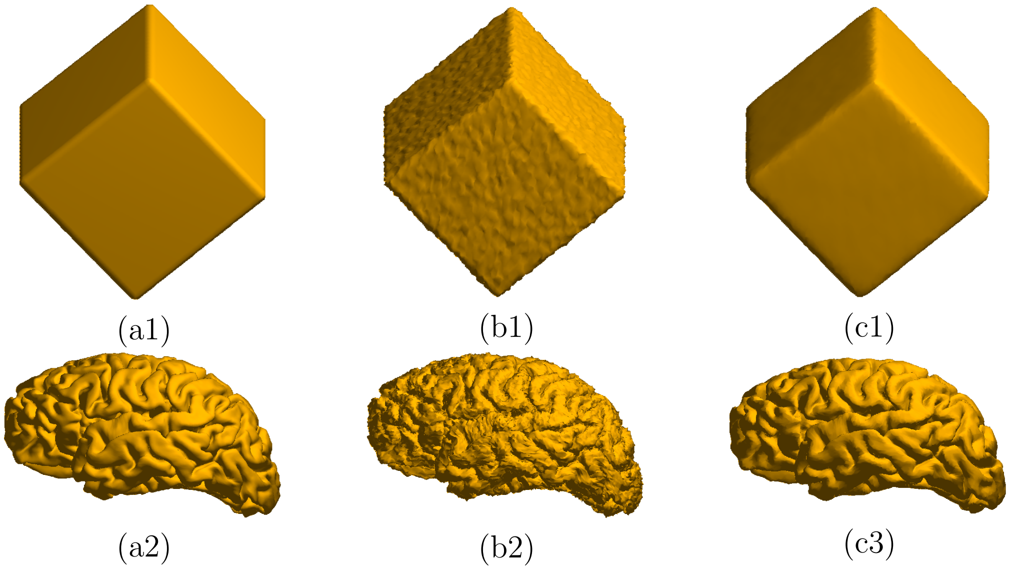

Figure 7: the first column: clean surfaces. the second column: noise surfaces with Gaussian noise $\sigma = 0.1$. the third column: denoised results obtained by split Bregman method.

7. Acknowledgement

This work is supported by NIH U54 RR021813, NSF IIS-0914580 and ONR N00014-09-1-0105. Authors would like to express their gratitude to Prof. Scott Fears for providing the vervet cortical surfaces database, their acknowledgement is further extended to the public databases ADNI, AIM@SHAPE and SHARP3D for their wonderful data supporting. The first author would like to specially thank all discussion with Prof. Luminita Vese, Prof. Yonggang Shi, Dr. Bin Dong, and Dr. Ernie Esser for their valuable suggestions to this work.

References

[1] Jean-Francois Aujol, Guy Gilboa, Tony Chan, and Stanley Osher. Structure-texture image decomposition - modeling, algorithms, and parameter selection. *Int. J. Comput. Vis.*, 67(1):111–136, 2006.

[2] Chandrajit L. Bajaj and Guoliang Xu. Anisotropic diffusion of subdivision surfaces and functions on surfaces. *ACM Transaction on Graphics*, 22(1):4–32, 2003.

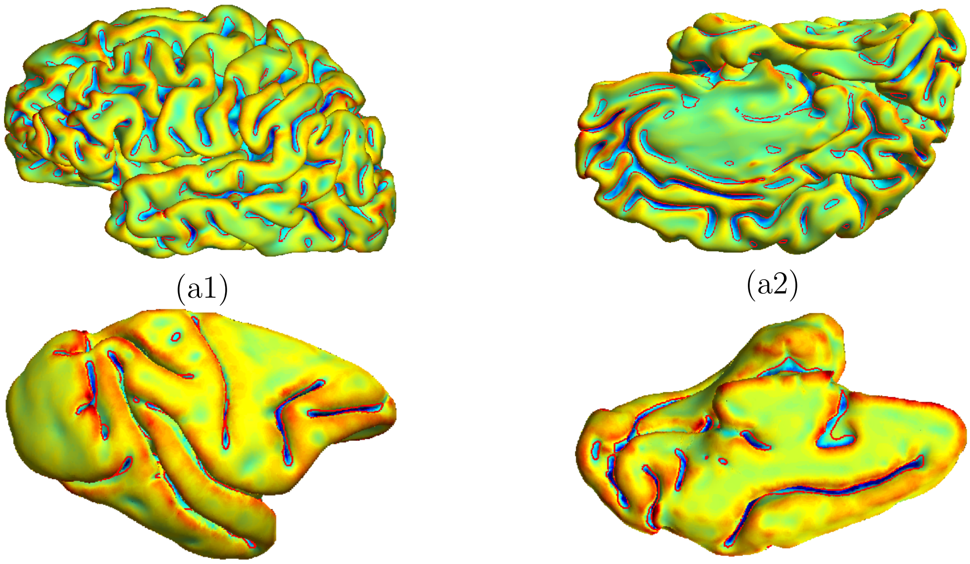

(a1) (a2)

(b1) (b2)

Figure 8: Top: Two different views of CCV segmentation on the mean curvature of a human's cortical surface. Bottom: Two different views of CCV segmentation on the mean curvature of a vervet's cortical surface. Surfaces are color coded with their mean curvature and the red contours mark the boundary of the sulcal and gyral regions.

[3] Matania Ben-Artzi and Philippe G. LeFloch. Well-posedness theory for geometry-compatible hyperbolic conservation laws on manifolds. *Ann. I. H. Poincaré*, AN 24:989–1008, 2007.

[4] M. Bertalmio, F. Memoli, L.T. Cheng, G. Sapiro, and S. Osher. Variational problems and partial differential equations on implicit surfaces. *UCLA CAM Report (02-17)*, 2002.

[5] Marcelo Bertalmio, Guillermo Sapiro, Li-Tien Cheng, and Stanley Osher. A framework for solving surface partial differential equations for computer graphics applications. *UCLA CAM Report (00-43)*, 2000.

[6] Xavier Bresson, Selim Esedoḡlu, Pierre vandergheynst, Jean-Philippe thiran, and Sanley Osher. Fast global minimization of the active contour/snake model. *J.Math Imaging Vis*, 2007.

[7] M. Burger. Finite element approximation of elliptic partial differential equations on implicit surfaces. *Computing and Visualization in Science*, 12(3):87–100, 2009.

[8] Jian-Feng Cai, Stanley Osher, and Zuowei Shen. Split bregman methods and frame based image restoration. *UCLA CAM Report 09-28*, 2009.

[9] Antonin Chambolle. An algorithm for total variation minimization and applications. *J. Math. Imag. Vis.*, 20:89–97, 2004.

[10] Tony Chan, Selim Esedoglu, and Mila Nikolova. Algorithms for finding global minimizers of image segmentation and denoising models. *SIAM Journal on Applied Mathematics*, 66:1632–1648, 2006.

[11] Tony Chan and Jianhong Shen. Mathematical models for local nontexture inpaintings. *SIAM J. APPL. MATH.*, 62(3):1019–1043, 2001.

[12] Tony Chan and Luminita Vese. Active contours without edges. *IEEE Transactions on Image Processing*, 10:266–277, 2001.

[13] Tony F. Chan and Jianhong(Jackie) Shen. *Image processing and analysis: variational, PDE, wavelet, and stocastic methods*. Society for Industrial and Applied Mathematic, 2005.

[14] Isaac Chavel. *Eigenvalues in Riemannian Geometry*. Academic press. INC, 1984.

[15] U. Clarenz, U. Diewald, and M. Rumpf. Anisotropic diffusion in surface processing. *In T. Ertl, B. Hamann, and A. Varshney, editors, Proceedings of IEEE Visualization 2000*, 2000.

[16] U. Clarenz, M. Rumpf, and A. Telea. Surface processing methods for point sets using finite elements. *Journal on Computers and Graphics*, 28:851–868, 2004.

[17] M. Desbrun, M. Meyer, P. Schröder, and A. Barr. Implicit fairing of irregular meshes using diffusion and curvature flow. *ACM SIGGRAPH*, 1999.

[18] M. Desbrun, M. Meyer, P. Schröder, and A. Barr. Anisotropic feature preserving denoising of height fields and bivariate data. *Graphics Interface*, 2000.

[19] M. Desbrun, M. Meyer, P. Schröder, and A. H. Barr. Discrete differential geometry operators in nd. *In Proc. VisMath'02 Berlin Germany*, 2002.

[20] Bin Dong, Jian Ye, Stanley Osher, and Ivo Dinov. Level set based nonlocal surface restoration. *MMS*, 7(2):589–598, 2008.

[21] I. Ekeland and R. Témam. *Convex Analysis and Variational Problems.* SIAM Classics in Applied Mathematics, 1999.

[22] M. Elsey and S. Esedoglu. Analogue of the total variation denoising model in the context of geometry processing. *UCLA CAM-Report 07(31)*, 2007.

[23] Ernie Esser, Xiaoqun Zhang, and Tony Chan. A general framework for a class of first order primal-dual algorithms for tv minimization. *UCLA CAM report(09-67)*, 2009.

[24] W. H. Fleming and R. Rishel. An integral formula for total gradient variation. *Arch.Math.*, 11:218–222, 1960.

[25] E. Giusti. *Minimal Surfaces and Functions of Bounded Variation.* Birkhauser, Boston, 1984.

[26] Tom Goldstein, Xavier Bresson, and Stanley Osher. Geometric applications of the split bregman method: Segmentation and surface reconstruction. *UCLA CAM Report 09-06*, 2009.

[27] Tom Goldstein and Stanley Osher. The split bregman method for l1 regularized problems. *UCLA CAM Report 08-29*, 2008.

[28] Xianfeng Gu and S.T.Yau. Global conformal surface parameterization. *Symposium on Geometry Processing*, pages 127–137, 2003.

[29] B. Merriman L.-T. Cheng, P. Burchard and S. Osher. Motion of curves constrained on surfaces using a level-set approach. *J. Comput. Phys.*, 175(2):604–644, 2002.

[30] Rongjie Lai, Yonggang Shi, Kevin Scheibel, Scott Fears, Roger Woods, Arthur W. Toga, and Tony F. Chan. Metric-induced optimal embedding for intrinsic 3d shape analysis. *Accepted, CVPR*, 2010.

[31] John M. Lee. *Riemannian Manifolds: An Introduction to Curvature.* Springer-Verlag, 1997.

[32] L. Lopez-Perez, R. Deriche, and N. Sochen. The beltrami flow over triangulated manifolds. *Computer Vision and Mathematical Methods in Medical and Biomedical Image Analysis*, 3117:135–144, 2004.

[33] L.M. Lui, X. Gu, T.F. Chan, and S.-T. Yau. Variational method on riemann surfaces using conformal parameterization and its applications to image processing. *Methods and Applications of Analysis*, 15(4):513–538, 2008.

[34] L.M. Lui, Y. Wang, T.F. Chan, and P.M. Thompson. Brain anatomical feature detection by solving partial differential equations on general manifolds. *Discrete and Continuous Dynamical Systems B*, 7(3):605–618, 2007.

[35] Lok Ming Lui. *Computational Conformal Geometry and Its Applications to Human Brain Mapping*. PhD thesis, UCLA, July 2008.

[36] G. Gimel'farb M. Krueger, P. Delmas. Active contour based segmentation of 3d surfaces. *In Proc. European Conference on Computer Vision (ECCV)*, pages 350–363, 2008.

[37] Mark Meyer, Mathieu Desbrun, Peter Schröder, and Alan H. Barr. Discrete differential-geometry operators for triangulated 2-manifolds. *Visualization and Mathematics III. (H.C. Hege and K. Polthier, Ed.) Springer Verlag*, pages 35–57, 2003.

[38] Stanley Osher, Martin Burger, Donald Goldfarb, Jinjun Xu, and Wotao Yin. An iterative regularizatoin method for total variation-based image restoration. *Multiscale Model. Simul.*, 4:460–489, 2005.

[39] L. Rudin, S. Osher, and E. Fatemi. Nonlinear total variation based noise removal algorithms. *Physica. D.*, 60:259–268, 1992.

[40] Y. Shi, Z. Tu, A. Reiss, R. Dutton, A. D. Lee, A. Galaburda, I. Dinov, P. M. Thompson, and A. W. Toga. Joint sulcal detection on cortical surfaces with graphical models and boosted priors. *IEEE Trans. Med. Imag.*, 28(3):361–373, 2009.

[41] J. Stam. Flows on surfaces of arbitrary topology. *Proceeding of ACM SIGGRAPH*, 22:724–731, 2003.

[42] Guoliang Xu. The convergent discrete laplace-beltrami operator over triangular surfaces. *Proceedings of Geometric Modelling and Processing*, pages 195–204, 2004.

[43] Mingqiang Zhu and Tony Chan. An efficient primal-dual hybrid gradient algorithm for total variation image restoration. *UCLA cam report (08-34)*, 2008.